Article

Nonuniform Woven Solar Shading Screens: Shading, Mechanical, and Daylighting Performance

Yao Lu, Hankun Lin, Siwei Liu and Yiqiang Xiao *

Faculty of Architecture, South China University of Technology, Guangzhou 510640, China;
luyao@scut.edu.cn (Y.L.); hklam@foxmail.com (H.L.); arliusiwei@gmail.com (S.L.)
* Correspondence: yqxiao@scut.edu.cn; Tel.: +86-020-87111321

Abstract: This study investigated the potential of using a nonuniform woven panel with nonuniform strips—thick sticks and thin battens—as an external solar shading screen that addressed daylighting, shading, and mechanical performance factors. The sustainable material, namely, bamboo, was used as the demonstration material for the screen. An on-site experiment and ANSYS simulation were carried out to investigate the basic solar optical performance and structural strength of the proposed screen, respectively. Then, a series of daylighting simulations were conducted to optimize the configuration of the screen. The results showed that the nonuniform woven solar shading screen reduced up to 80.3% of the solar radiation gain in a room during summer months while ensuring a relatively even distribution of useful daylight during the year. Moreover, the screen effectively reduced the negative impact of glare to a level below "imperceptible" and enabled a relatively clear view through the window and shading. Regarding the structural strength, the screen with a size smaller than or equal to 1 × 1 m withstood a wind load of 12 m/s. Furthermore, this study proposed two optimal configurations: a screen woven of square sticks and battens with a distance of 10 mm between them, and a screen woven of round sticks and battens with a distance of 8 mm between them. This study illustrated the superiority of the nonuniform woven solar shading screens, which supports a wider application of solar shading screens made of other materials with similar structures and reflectance values.

Keywords: nonuniform woven panel; solar shading screen; bamboo; solar optical properties; structural strength; daylighting performance

1. Introduction

Optimized building skins can significantly reduce energy consumption for space heating, cooling, and electric lighting [1,2]. Using solar shading systems for natural cooling and daylighting control is an extensively researched topic in the area of energy-efficient building design [3,4]. Specifically, solar shading systems contribute significantly to controlling glare, regulating solar radiation, homogenizing illuminance levels, and protecting privacy [5,6]. On the basis of spatial positions, solar shading devices can be divided into three categories, namely, external intermediate and intermediate shading systems [7]. Many studies have demonstrated that external shading presents a better solar shading performance than internal and intermediate shading [8,9]. Regarding the operable and geometrical property, current solar shading systems consist of the fixed solar shading screen, fixed overhang, grating, operable solar shading screen, Venetian blinds, shutters, and roller blinds [10,11]. As one of the most commonly used external shading devices, a solar screen can efficiently scatter and redirect daylight [12]. Numerous studies have been conducted on improving the shading performance of solar screens by optimizing their geometrical dimensions, perforation percentages, and textures [13–15]. Moreover, much research has been conducted on

using solar screens more effectively by adjusting their application methods on the basis of the facade orientation and shading periods [16]. Conventional research on the performance evaluation of shading devices has primarily focused on standard solar transmission (e.g., solar heat gain coefficient) and visible daylight transmittance [17,18]. At present, concerns regarding the overall daylight quality of the indoor environment in a room with different shading devices have been increasing [19–21], and the research methods have been expanded to a wider range of simulations, regarding daylight, visual comfort, and energy demand, by using climate-based computer-aided dynamic simulation tools [22–24]. On the basis of the methods above, the performance of various kinds of materials for solar screens has been investigated, including metal mesh grids, perforated metal screens, and wooden screens [25–27]. The distinctive light performance of a woven fabric was demonstrated by Thomas in 1967. He demonstrated that the daylight transmission process of the woven fabric includes transmission through the holes, reflection by the fibers, and diffraction [28]. Likewise, mats woven of fine strips (e.g., rattan mats, bamboo mats) have a similar daylight transmission mechanism as fabric materials, which allows them to be developed into daylighting/shading devices. These mats can provide a preferable daylight transmission performance and combine aesthetics and functionality by delivering a striking visual appeal, safety, and energy savings.

However, as is shown in Figure 1a, traditional uniform woven mats show relatively weak shading performance because their thin warp and weft strips cannot significantly reduce direct solar radiation. In contrast, as shown in Figure 1b, conventional thick perforated panels effectively block the direct solar beam but limit the access of diffuse daylight. The weaknesses of the aforementioned panel types necessitate the search for an alternative material for solar screens. To address this problem, this paper proposed a nonuniform woven panel woven from strips of different thicknesses. The thick strips function as the main component to obstruct direct solar beams, whereas the side openings formed by curved thin strips allow almost exclusively diffuse daylight to penetrate. In this study, bamboo was used as a demonstration material for the screen. Due to the toughness and tensile strength of bamboo, fine strips can be easily curved and woven into mats with different patterns in the same way as fabrics [29,30]. In terms of the raw material itself, the ecology potentials of bamboo as an environmentally friendly resource have been an increasingly considered option in the field of renewable building materials [31–33]. Bamboo is widely planted and utilized as industrial or building material in Southern and Southeast Asia [34]. This material has a number of eco-features, such as rapid growth, a short vegetative cycle, and low-cost cultivation [35]. For example, Phyllostachys pubescen can grow to a height of 18 m in only 59 days after felling [36]. Bamboo products have lower eco-costs than tropical hardwood alternatives [37]. In addition, varied woven patterns endow mats with special aesthetic appearances for the envelope components [38,39]. Thus, the distinctive characteristics of bamboo warrant an investigation of the nonuniform solar shading screen that simultaneously takes into account the daylighting performance and eco-features of bamboo. To the best of our knowledge, this panel has not been used as an external shading device, and no quantitative analysis has been conducted on its shading, daylighting, and mechanical performance.

This study, therefore, aims to determine the potential application of the proposed woven panel as an external solar shading screen on a south façade by comprehensively assessing the solar optical properties, structural strength, and overall indoor performance. To this end, the following two research questions will be addressed: (1) What are the daylighting, solar optical properties, and the wind load performance of the nonuniform woven bamboo panel when used as an external shading device? (2) What optimizations of the configuration can be made to balance the daylighting, visual, and solar shading performance? This study not only provides insight into the material properties, but also focuses on the overall annual performance of the shading screen at a room scale. Moreover, the mechanical performance of the structure was simulated to quantify the strength in practice. Notably, materials for the nonuniform woven solar shading screens included but were not limited to bamboo. All materials had similar optical and mechanical properties to bamboo and were suitable for solar shading screens, which indicate a broader range of applications with respect to building skins.
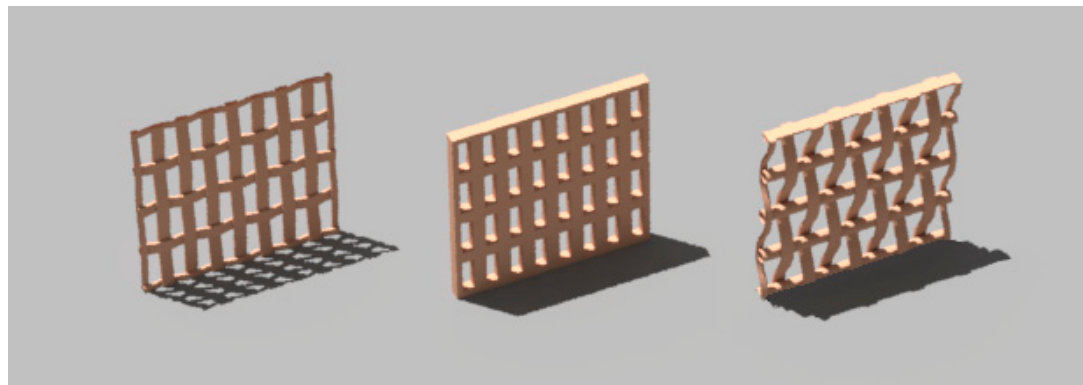
(**a**)
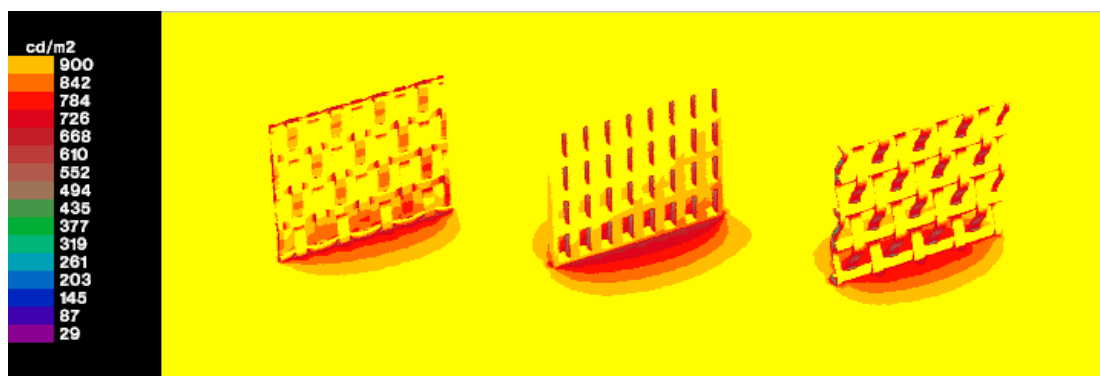
(**b**)

Figure 1. Comparison of the shading effects of different solar screens for direct and diffuse daylight. (**a**) The Radiance rendered image of shading performance under clear sky with direct solar radiation. Left: traditional thin woven mat; middle: thick perforated panel; right: nonuniform woven panel. (**b**) The false color image of the illuminance distribution under an overcast sky with diffuse solar radiation. Left: traditional thin woven mat; middle: thick perforated panel; right: nonuniform woven panel.

2. Methods

This study consists of two steps, as follows:

Step 1: Basic property investigation. The investigation in this part contained three parts: First, an experiment and a simulation in a test box were conducted for the visible daylight transmittance and the solar radiation transmittance of the proposed woven bamboo panel on a typical summer day. Second, simulations in a residential room were conducted for the daylighting performance on a typical summer day and the glare performance on both a typical summer and an autumn day. The view performance was investigated using an on-site photograph in a test room. Third, the bending strength against a wind load of the proposed panel was simulated under 42 different wind pressures with 6 levels from 7 wind directions.

Step 2: Configuration optimization. To select the best overall performing configurations, 18 varieties of solar shading screens with different batten distances and stick section forms were analyzed. The optimization considered not only the solar shading performance of the screens, but also the daylighting performance of a room applying the screens. Accordingly, the annual daylighting, glare, and radiation shading performance in a residential room with different screens were simulated and cross-compared.

2.1. Study Object

As shown in Figure 2a, the proposed solar shading screen panels were woven bamboo battens and sticks interlaced at right angles. The thickness of all the battens was 1 mm. The thickness of the sticks was five times greater than that of the battens. The sections of the sticks consisted of two types: square and round. The specific configurations and material parameters of the screen panels used for different steps were as follows:

- Step 1: The panel was formed by the battens and square sticks, and the distance between each batten (d) was 5 mm. The raw material of the panel was Phyllostachys pubescens, and its modulus of elasticity, Poisson's ratio, and density were 9.4432×10^9 Pa, 0.36, and 542 kg/m^3, respectively. The maximum tensile strength and compressive strength (σp) along the grain were 1655.2 kg/cm^2 and 445.7 kg/cm^2, respectively. The safety coefficient (n) was 1.5. Thus, the allowable stress of the panel in this study was $\sigma a = \sigma p/n = 297.1$ kg/cm^2 = 29.71 MPa.
- Step 2: As shown in Figure 2b, panels for the optimization were divided into two groups: panels with square sticks (thickness = 5 mm) and panels with round sticks (diameter = 5 mm). Each group had nine varieties with different d values, which were 5 mm, 6 mm, 7 mm, 8 mm, 9 mm, 10 mm, 11 mm, 15 mm, and 20 mm.
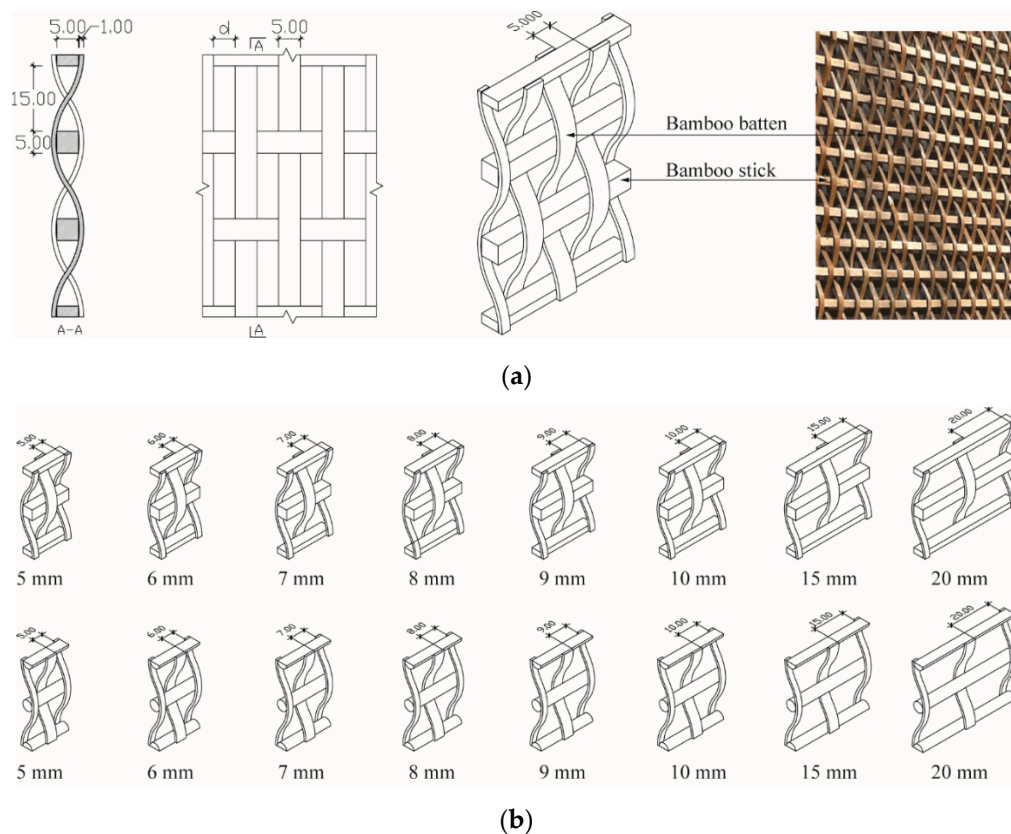

(**a**)

(**b**)

Figure 2. Schematic diagram of the structures and configurations for the nonuniform woven solar shading screen. (**a**) Structure of the solar shading screen made of bamboo. (**b**) Optimization varieties with two types of sticks and different distances between each batten.

2.2. Evaluation Indicators

The evaluation indicators in each step were as follows:

- Step 1: Horizontal and vertical visible daylight transmittances (τ_{vh} and τ_{vv}) in each daylighting hour on 21 June were used to evaluate the daylight access ability. The direct solar radiation

transmittance (τ_{sdir}) and diffuse solar radiation transmittance (τ_{sdif}) were treated separately to assess the solar radiation control property. The indoor daylighting performance was evaluated on the basis of the hourly mean horizontal illuminance (E_{vm}) on 21 June. The indicators used to evaluate glare were the daylight glare probability (DGP) and glare level (GL) at 9:00 and 12:00 on 21 June and 21 September. Four glare levels were classified: imperceptible (DGP < 35%), perceptible (40% > DGP ≥ 35%), disturbing (45% > DGP ≥ 40%), and intolerable (DGP ≥ 45%). A view photograph was used to evaluate the view quality. The evaluation indicators for the mechanical performance were the plane normal deformation and the axial bending stress (σ_b) of the panel structure under wind loads.

- Step 2: The evaluation indicators for the daylighting performance included the daylight factor (DF) and useful daylight illuminance ($UDI_{100-2000}$). On the basis of the daylighting standard for residential buildings in China [40], the minimum required DF is 2%; thus, in this study, 2% was selected as the baseline for the daylighting level. The indicator for visual comfort was the annual daylight glare probability (aDGP). The evaluation indicators for solar shading performance were the monthly solar radiation transmittance (τ_{smon}) and the monthly total solar insolation (Q_s).

2.3. Study Tools and Simulation Setup

2.3.1. On-Site Experiment in a Test Box in Step 1

The on-site experiment was conducted in a test box at the Solar Station of TU Munich, as shown in Figure 3a. The test box was located on the roof of a five-story building in Munich, Germany (latitude 48°09′ N, longitude 11°34′ E). It was possible for it to be rotated along the horizontal or vertical axis to adjust the solar elevation angles and azimuth angles. The net size of the box was 1500 × 1000 × 1500 mm (width × height × depth). The window in the southern wall was 1465 × 1103 mm and had a single glazing. The texted solar shading screen was made up of six woven bamboo panels (500 × 500 mm) connected by hinges. The width of the wooden frames of each panel was 20 mm. The solar shading screen was installed outside the window and covered the glazed part of the window. The radiance materials and the relative parameter values of surfaces, glazing, and solar shading screens are shown in Table 1. A light meter (LX1010BS) was used to measure the illuminance.

Table 1. Materials and radiance parameters of the room surfaces and shading screens.

Surface	Vertical Surfaces of the Test Box/Room Walls	Lower Horizontal Surface of the Test Box/Room Floor	Upper Horizontal Surface of the Test Box/Room Ceiling	Window	Solar Shading Screen
Material	White plaster	Fine concrete	White plaster	Single glazing	Bamboo
Reflectance	50%	20%	70%	-	0.5, 0.3, 0.2 (red, green, blue)
Transmittance	0	0	0	90%	0

The on-site test was conducted on 18 July, from 8:00 to 18:00 under a clear sky. As the study investigated the application of woven bamboo panels in China, the box was adjusted hourly in line with the solar elevation angles and azimuth angles on a typical summer day, namely, 21 June in Xi'an, China (latitude 34°14′ N and longitude 108°56′ E). The horizontal ambient illuminance at 12:00 was 11,2500 lx. A total of 10 test points for E_{vho} were set outside the room forming the middle line of the solar shading screen. Another 10 measurement points for E_{vhi} were set inside the room to form the middle line of the window. The interval between each point was 100 mm. The frequency of readings was every hour. The view photo was taken 1.5 m away from the window at a height of 750 mm at 12:00.

2.3.2. Simulations for the Solar Optical Properties of the Solar Screen in Step 1

DIVA-for-Rhino version 3.0 was used as the simulation tool. The model was built in accordance with the on-site test box and the solar shading screen located on it. To calculate τ_{vh}, E_{vhi} and E_{vhi}

were simulated on different grid surfaces. As shown in Figure 3b, for E_{vhi}, 10 narrow horizontal grid surfaces were placed inside the room next to the window, whereas for E_{vhi}, the other 10 were placed outside the room in front of the shading screen. Each grid surface was 1500 × 50 mm. The distance between each calculation node was 10 mm. To calculate τ_{vv}, two vertical grid surfaces for E_{vvi} and E_{vvo} were set up: one was inside the room behind the window, and the other was outside the room in front of the shading screen. The vertical test surface area was equal to the window area.
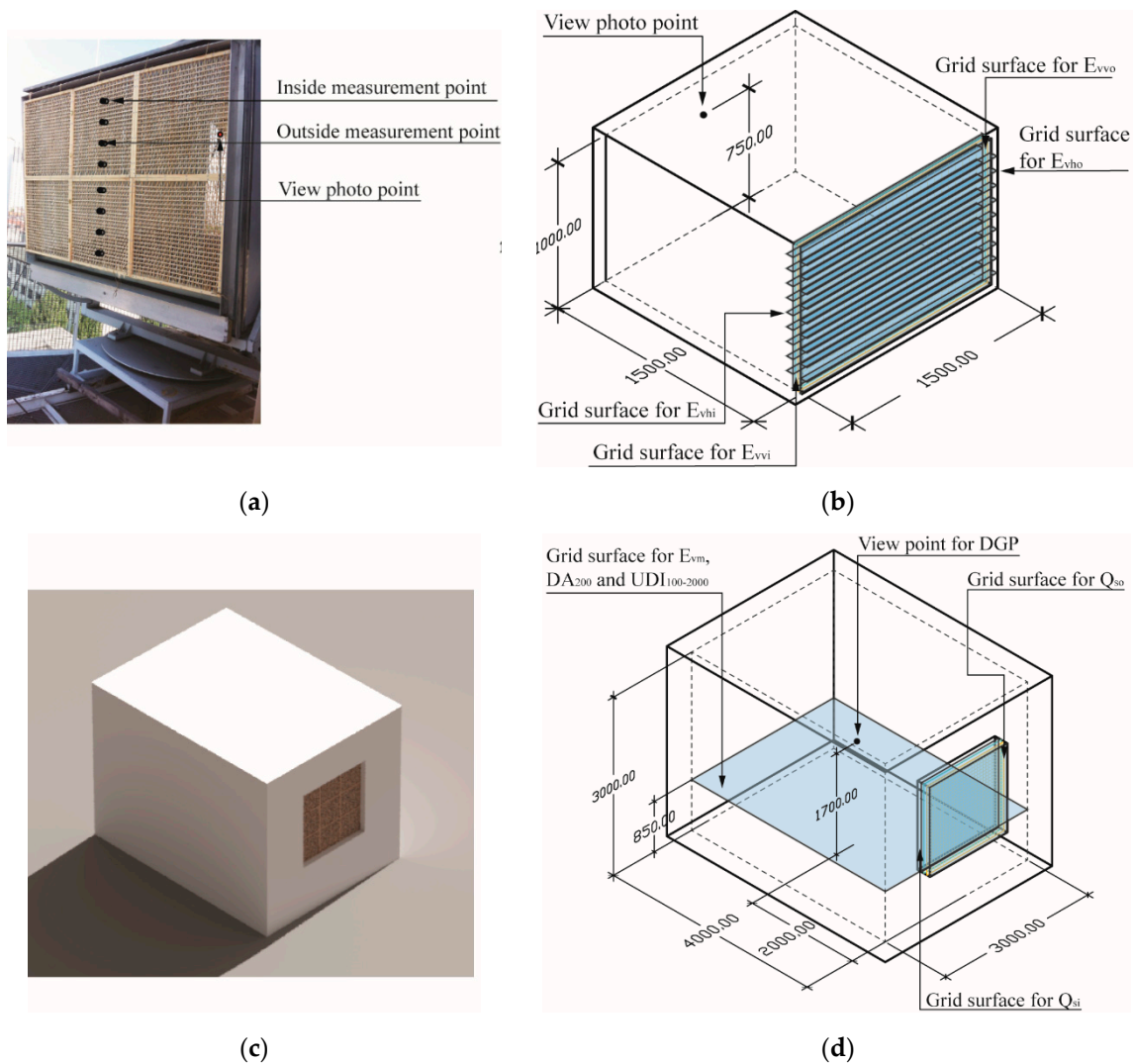

(a)

(b)

(c)

(d)

Figure 3. Perimeters, test surfaces, and test points in the on-site experiment and simulation models. (**a**) The test box in the solar station for the on-site experiment. (**b**) Test box model in the simulation. (**c**) Simulation model of a residential room rendered using Radiance. (**d**) Room model in the simulation. DGP: daylight glare probability.

2.3.3. Simulations for the Daylight and Shading Performance in a Room in Steps 1 and 2

The simulation tool was also DIVA-for-Rhino version 3.0. The evaluations of daylighting and shading performances were conducted by simulating a typical residential room with different varieties of the proposed solar shading screen. As shown in Figure 3c, the room was 3000 × 3000 × 4000 mm (width × height × depth). The window located on the south facade was 1500 × 1500 mm and was completely covered by the solar shading screen. The materials of the room surface, glazing, and solar shading screen were set as the values in Table 1. The CSWD (Chinese standard weather data) weather file of Xi'an in China was used as the climate data. The reference room for the comparative study was

the same room but had a clear, unshaded single glazed window. The simulation sensor points or grid surfaces for the different evaluation indicators were set as follows (see Figure 3a,b for details):

To simulate Q_{si} and Q_{so}, (which were used to calculate the τ_{sdir}, τ_{sdif}, and τ_{smon}), two vertical grid surfaces were set. One grid was placed just behind the window surface inside the room (for Q_{si}), while the other grid was just in front of the shading panel (for Q_{so});

To simulate the DGP, a viewpoint was set at a height of 1700 mm and 2 m away from the window;

To simulate the E_{vm}, DF, and $UDI_{100-2000}$, a horizontal grid surface was placed at a height of 850 mm above the floor with a grid size of 50 mm.

2.3.4. Simulation for Mechanical Performance in Step 1

To evaluate the mechanical performance of the panel under different wind loads, the wind velocity (v_w) varied from 2 m/s to 12 m/s with an interval of 2 m/s, on the basis of the wind rose plot (from CSWD) in Xi'an, China. The wind direction angle was defined as the angle between the wind direction and the surface, ranging from 0° to 90°, having an interval of 15°. The wind load can be calculated by Equation (1).

$$q_w = \frac{1}{2} \rho_a v_w^2, \tag{1}$$

where q_w is the wind pressure (kN/m^2), ρ_a is the air density (kg/m^3), and v_w is the wind velocity (m/s). The relationship between ρ_a and air gravity (W_a) can be seen in Equation (2):

$$\rho_a = \frac{w_a}{g}. \tag{2}$$

The parameters used for the calculation were as follows: atmospheric pressure = 1013 Pa, temperature = 15 °C, w_a = 0.01225 kN/m^3, and g = 9.8 m/s^2. On the basis of Equations (1) and (2), the wind load can be calculated using Equation (3):

$$q_w = \frac{v_w^2}{1600}. \tag{3}$$

The finite element software ANSYS was used to calculate the bending stress and the normal deformation of the panel under wind loads. All degrees of freedom on the four edges of the panel were constrained. The beam element—beam 188—was used to simulate the entire structure. The panel was divided into 60,447 elements with 76,097 nodes. The finite element model is shown in Figure 4.
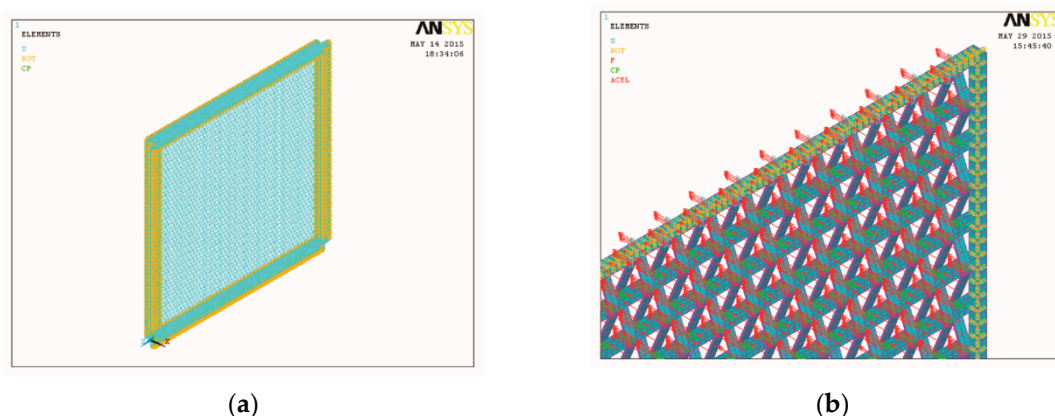

(a)   (b)

Figure 4. Finite element model of the woven bamboo panel. (**a**) Finite element model of the panel. (**b**) Diagram of the wind load and boundary constraint.

3. Results Part 1—The Basic Performance of a Nonuniform Woven Bamboo Panel

3.1. Visible Daylight Transmittance

Figure 5a demonstrates the variations in the hourly horizontal visible daylight transmittance calculated by the hourly illuminance from the on-site experiment and computer simulation on 21 June. In both the measured and simulated results, the τ_{vh} values in the early morning and late afternoon were much greater than those at other daylight time points. The dramatic change in τ_{vh} values during the day was caused by the fact that before 10:00 and after 16:00, the solar azimuth angle was less than 90° or greater than 270°. No direct daylight fell on the southern facade during these time points. Thus, the τ_{vh} values during these periods indicated the horizontal diffuse daylight transmittance. In contrast, the τ_{vh} values between 10:00 and 16:00 indicated the horizontal total daylight transmittance. The lower the horizontal total daylight transmittance was, the better its shading performance.
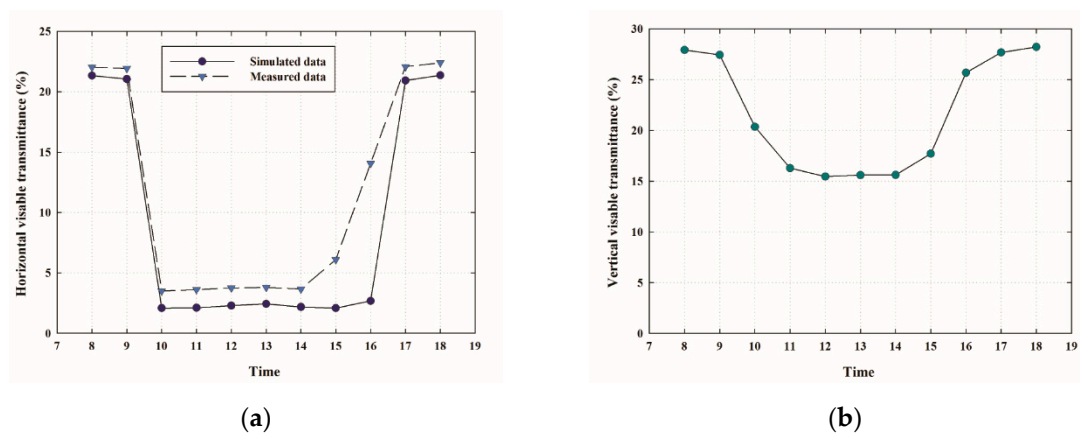

Figure 5. Horizontal and vertical visible daylight transmittances. (**a**) Horizontal visible daylight transmittances using a test and a simulation. (**b**) Vertical visible daylight transmittance using a simulation.

On the basis of the on-site experiment, the τ_{vh} values between 10:00 and 14:00 ranged from 3.49% to 3.80%, and those at the time points before and after this period ranged from 21.93% to 22.40%. The simulation showed that these ranges were 2.08% to 2.68% and 20.93% to 21.37%. These ranges indicated that the proposed solar shading screen applied to the south facade could effectively block direct visible daylight and ensure that approximately 21% of horizontal diffuse daylight penetrated the room in a summer day, which is also advantageous in maintaining a continuous soft indoor daylight throughout the day.

Regarding the validation of the simulation tool, Figure 5a shows that the simulation results of the diffuse horizontal visible daylight transmittance values were in good agreement with the test results, as the relative deviation was only 4.8%. Major differences were found at 17:00 and 18:00 due to the error in adjusting the solar elevation angle and azimuth angles in the on-site test; thus, the test results at these two measurement hours could not be compared. Accordingly, the simulation was reliable and was used in the remainder of this study.

Figure 5b shows the hourly vertical visible daylight transmittance based on the simulation. The smallest τ_{vv} was 15.46% at 12:00, whereas the greatest τ_{vv} was 28.22% at 18:00. Compared with the horizontal surface, a greater proportion of diffuse daylight fell on the vertical surface in front of the shading panel at noon on 21 June, and thus the smallest τ_{vv} was greater than the smallest τ_{vh}. The result demonstrated that the proposed solar shading screen applied on the south facade blocked all the direct vertical daylight and ensured that approximately 28% of the diffuse vertical daylight penetrated into the room on the summer solstice day.

3.2. Solar Radiation Transmittance

Figure 6 displays the solar radiation transmittance of the proposed panel over a year. In terms of direct solar radiation transmittance, the smallest τ_{sdir} was 0, which was the case in the months of May, June, and July, whereas the greatest and second greatest τ_{sdir} were 19.59% and 18.79%, which were the case in the winter months of December and January, respectively. The τ_{sdir} values declined sharply during the transition from winter to spring and reached the lowest point in summer, then increased again in the transition from autumn to winter. For diffuse solar radiation transmittance, the values of τ_{sdif} showed a relatively flat curve from February to October, where the average τ_{sdif} value was 21.20%. The τ_{sdif} values in November, December, and January, ranging from 27.17% to 31.15%, were greater than those in other months. The results above revealed that the proposed panel effectively controlled the access of solar energy in summer, whereas it enabled high passive solar energy heating during winter. This property helped to reduce cooling and heating energy consumption. Furthermore, when the distance between each horizontal stick was 15 mm, the direct daylight could be significantly reduced in summer; thus, 15 mm was selected as the distance between the sticks for all the varieties below.
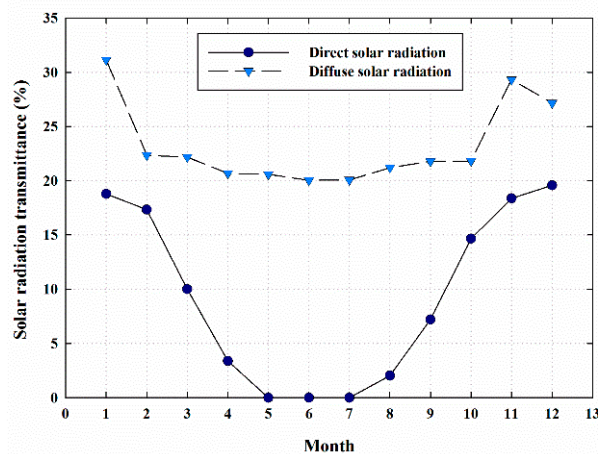

Figure 6. Direct and diffuse solar radiation transmittance.

3.3. Mean Illuminance and Daylight Factor

Figure 7 presents the hourly mean illuminance on the working plane surface in the reference room without a shading screen and in the room with the proposed shading screen on 21 June. For the reference room, the E_{vm} values varied from 721.35 to 2384.63 lx, and the difference between the highest and lowest values was 1663.28 lx. For the room with the shading screen, the E_{vm} values varied from 160.08 to 451.11 lx, and the difference between the highest and lowest values was 291.03 lx. The indoor daylight changed much less dramatically than the reference room and was kept at a relatively stable level over a day. However, the E_{vm} values at 8:00 and 18:00 were 186.50 and 160.08 lx, respectively, which is relatively dark for a residential room. A further simulation showed that the daylight factor of the room with the shading screen was only 1.31%, which is lower than the required daylight factor (2%) for a living room and bedroom according to Chinese standards. Thus, an optimization of the solar screen configuration was necessary for better daylighting performance.

3.4. Glare and View

Figure 8a,b illustrates the glare distributions and the DGP of the room with the proposed solar shading screen observed from the center of the room at 9:00 and 12:00 on 21 June and 21 September. The DGP values ranged from 28% to 25%, indicating that all the glare levels at the test time points could be classified as "imperceptible". The DGP values of the reference room without shading are presented in Figure 8b. Only at 9:00 on 21 June could the glare stay at the "imperceptible" level, whereas the

glare levels at the other three test time points were "perceptible" (at 12:00, 21 June; 9:00, 21 September; and 12:00, 21 September) or even "disturbing" (at 12:00, 21 September). The reduction rate of DGP using the proposed shading screen ranged from 33.3% to 19.4%. Hence, the proposed shading screen can significantly reduce harmful glare and improve indoor visual comfort.
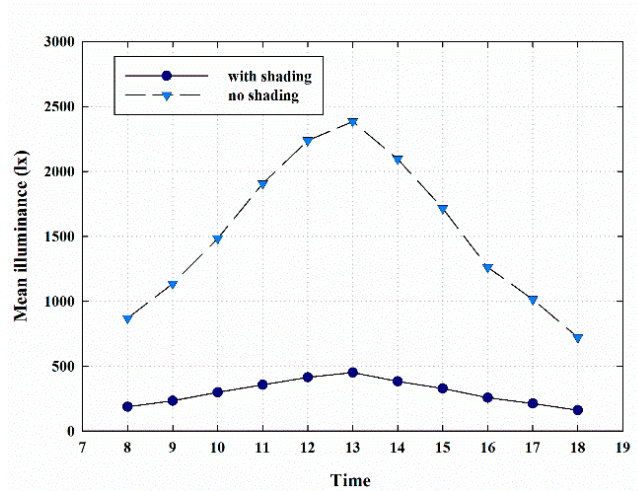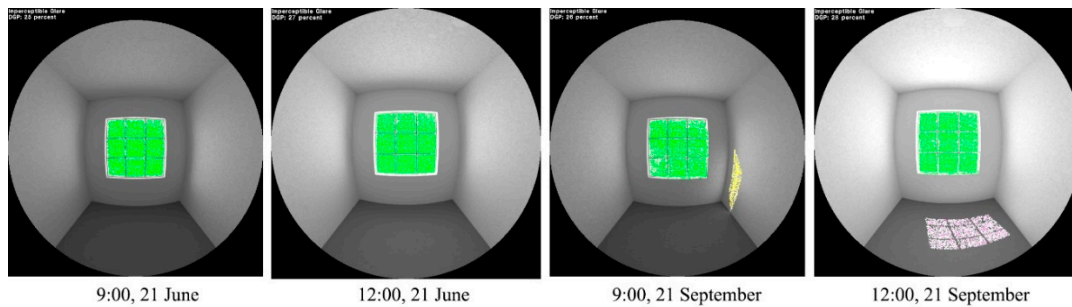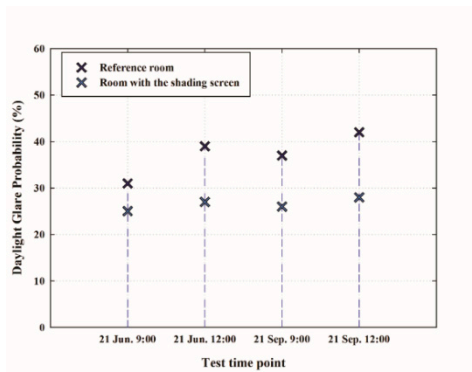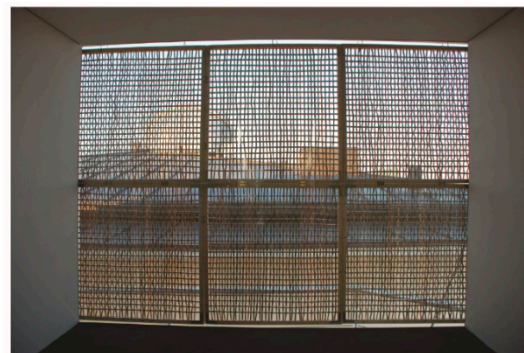

Figure 7. Comparison of the hourly mean illuminance in rooms with and without the nonuniform bamboo woven solar shading screen.

(**a**)

(**b**)

(**c**)

Figure 8. Glare analysis and view outside. (**a**) Fish-eye view images of a room with a solar shading screen for point-in-time glare distribution. (**b**) DGP at different test time points. (**c**) View through the window and solar shading screen.

Figure 8c illustrates the view looking straight through the window and shading screen from the interior of the test box at 12:00 on 21 June. The results showed that solar shading affected the

clarity of the view outside; however, this obstruction did not prevent observers from seeing the buildings and landscapes outside, and thus the observers had a sense of connection with the outside environmental conditions.

3.5. Mechanical Performance

Figure 9a presents the deformations of the proposed panel in the normal direction and the axial bending stress distributions under the maximum wind speed of 12 m/s with a wind direction angle of 0°. The maximum deformation value was 6.43 mm, which was located at the center of the structure. As the structural rigidity of the thick sticks was much higher than that of the thin battens, the maximum bending stress occurred at the end of the sticks (see Figure 9b for details). The maximum axial bending stress of the panel structure was 5.41 MPa, which was much lower than the allowable stress (29.71 MPa).
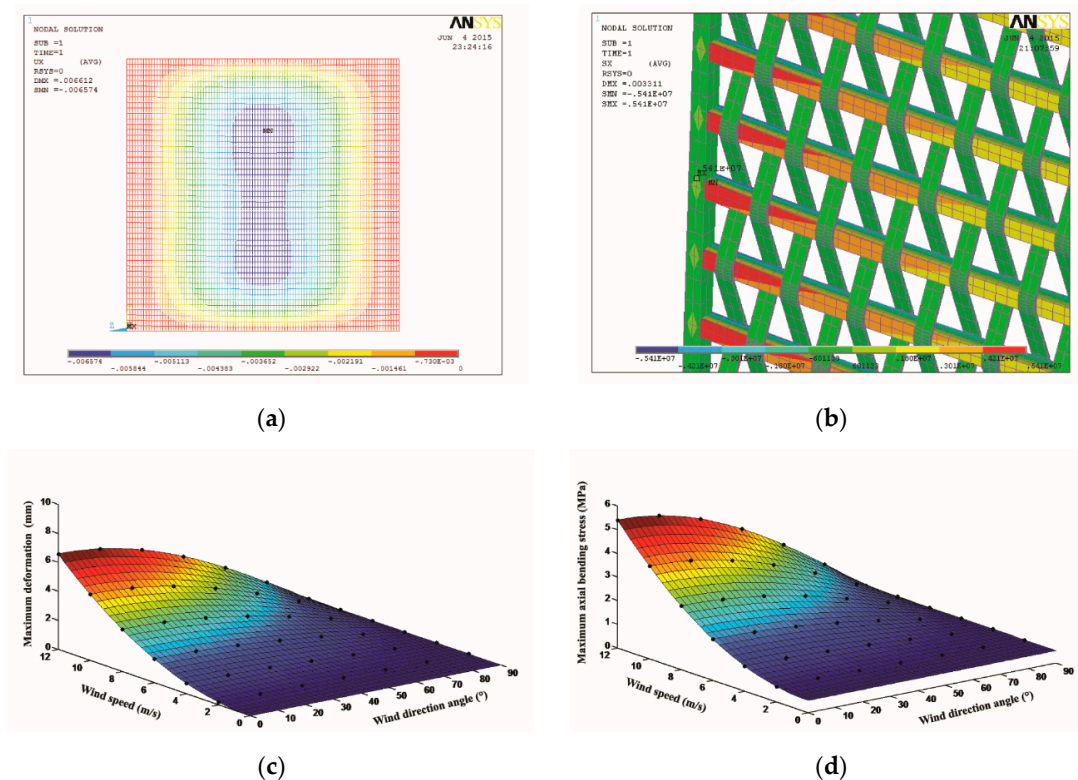

(a)

(b)

(c)

(d)

Figure 9. Finite element simulation results. (**a**) Deformation distribution. (**b**) Stress distribution. (**c**) Maximum normal deformation with a wind load. (**d**) Maximum stress with a wind load.

On the basis of the simulation results, the variations in the maximum axial bending stress and the maximum deformation under different wind loads with different wind directions were recreated in two surface plots (see Figure 9c,d, respectively, for details). The figures showed that the maximum axial bending stress of the thick sticks and the maximum deformation of the structure increased rapidly with increasing wind speed and decreased with increasing wind direction angles. Under all conditions, the maximum axial bending stress was much lower than the allowable stress, and the maximum deformation was within the acceptable range. Thus, the structure of the proposed panel met the requirements of strength and stiffness with regard to the wind load.

4. Results Part 2—Configuration Optimization for the Nonuniform Woven Shading Screen

The previous section focused on the basic performance of a nonuniform woven bamboo panel. In this section, the configuration of the proposed nonuniform woven shading screen is optimized, with the objective of an optimal structure with well-balanced performance. The results in this part

facilitate a wider range of application values for other kinds of nonuniform woven shading screens with similar structures.

4.1. Annual Daylighting Performance

The daylight factor (DF) and useful daylight illuminance ($UDI_{100-2000}$) of the solar shading screens woven of square sticks or round sticks with different distances (d) are displayed in Figure 10a–d. For all the varieties, the DF values increased significantly with increasing d values, whereas the $UDI_{100-2000}$ values decreased with increasing d values. Thus, to balance the indoor brightness and visual comfort, the best overall-performing d value should be the one that ensures the required DF (2%) but achieves the highest $UDI_{100-2000}$ possible.
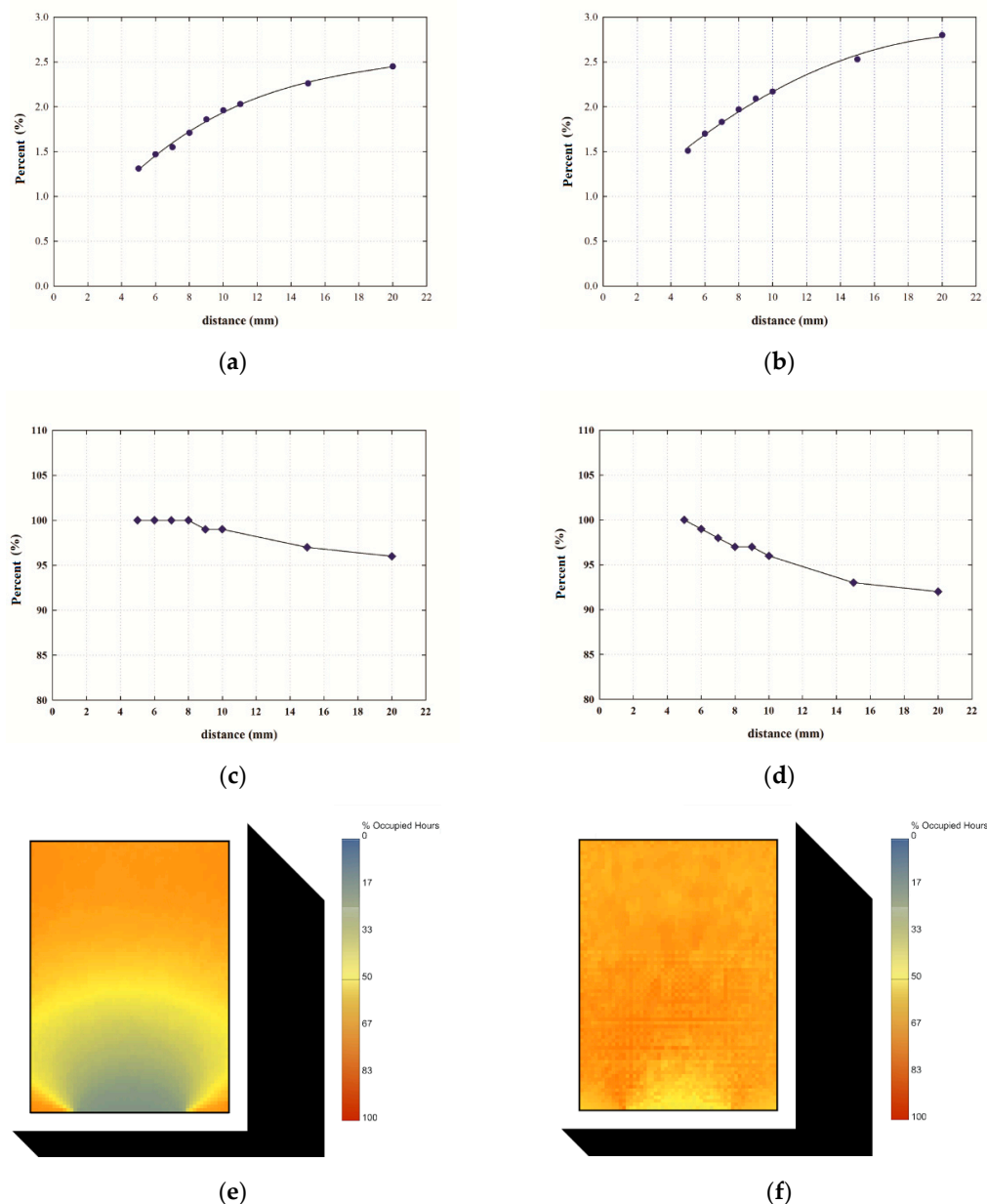

(a)

(b)

(c)

(d)

(e)

(f)

Figure 10. Daylight factor (DF) and $UDI_{100-2000}$ for solar screens with different stick sections and batten distances. (**a**) DF for the screens with square sticks. (**b**) DF for the screens with round sticks. (**c**) $UDI_{100-2000}$ for the screens with square sticks. (**d**) $UDI_{100-2000}$ for the screens with round sticks. (**e**) $UDI_{100-2000}$ distribution in the reference room. (**f**) $UDI_{100-2000}$ distribution in the room with a nonuniform woven solar shading screen using square sticks, d = 10 mm.

For screens with square sticks, Figure 10a,c show that when the d value was 10 mm, the DF value reached 2%, and the corresponding $UDI_{100-2000}$ value was 99%. Figure 10b,d presents the DF and $UDI_{100-2000}$ values of the screens with round sticks. Compared with square sticks, the curves of DF and $UDI_{100-2000}$ reviewed a similar trend, but showed a better performance in DF and a worse performance in $UDI_{100-2000}$ for the same d value. In terms of the overall performance, when the d value was greater than 8 mm, the DF value was greater than 2%, and the corresponding $UDI_{100-2000}$ value was 97%.

Figure 10e,f illustrate the $UDI_{100-2000}$ distributions on the grid surfaces in the reference room and the room with a better-performing solar screen that was woven of square sticks with a d value of 10 mm, respectively. As was evident, the solar screen efficiently reduced the over-lit area in the perimeter zone and created a relatively even distribution of useful daylight throughout the room during the whole year.

In summary, solar shading screens with round sticks enabled a larger amount of daylight access than those with square sticks. For screens with square sticks, the d value of 10 mm led to a relatively better overall performance in terms of both DF and $UDI_{100-2000}$, whereas this value was 8 mm for screens with round sticks.

4.2. Annual Glare

Figure 11a,b shows the hours of the DGP values that fell within the four glare classes for one year for the reference room and the rooms with eight varieties of woven solar shading screens. The eight varieties were screens with square sticks (d = 5, 10, 15, 20 mm) and screens with round sticks (d = 5, 10, 15, 20 mm). The total daylight hours in one year was 3896. For the reference room, the "imperceptible" and "perceptible" glare hours were 2471 and 485 h, respectively, whereas the "disturbing" and "intolerable" glare hours were 381 and 559 h, respectively. When using any of the proposed shading screens, the "intolerable" glare disappeared. The "disturbing" glare hours were reduced to less than 48 h per year. Compared with the reference room, the percentage of "imperceptible" glare hours in total annual daylight hours was improved from 63.4% to more than 91.4%. For the same d value, screens with square sticks produced less glare than those with round sticks. For all shading screens, the hours of "imperceptible" glare decreased as the d value increased. No "disturbing" or "intolerable" glare appeared when the d values were less than 10 mm. Therefore, the glare caused by all the shading screens was acceptable, and those with a d value that was less than or equal to 10 mm were more preferable.

Figure 11c,d shows the annual glare for the reference room without shading and the room with a better performing solar shading screen for glare control, which was woven from square sticks with a d value of 10 mm. For the reference room, the harmful glare at the "disturbing" and "intolerable" levels occurred frequently between 12:00 and 16:00 almost every day of the year. For the room with the proposed solar shading screen, the glare was maintained at the levels of "imperceptible" or "perceptible". In particular, during the months from April to September, the glare remained at the "imperceptible" level only. Accordingly, the proposed shading screen significantly reduced the annual glare.

4.3. Solar Radiation Transfer

Figure 12a,b shows the monthly amount of solar insolation that penetrated the rooms with different shading screens. For both types of screens, the largest solar insolation value in each month (Q_{smon}) appeared at d = 20 mm, which was 1.7 times as large as the smallest value in the same month, appearing at d = 5 mm. The solar shading screens with round sticks allowed more solar radiation to penetrate the room compared with those with square sticks. In particular, when the d value was 5 mm, the difference in the annual solar insolation between these two types of screens was 18.93 kWh/m^2, whereas when the d value was 20 mm, the difference was 33.41 kWh/m^2.
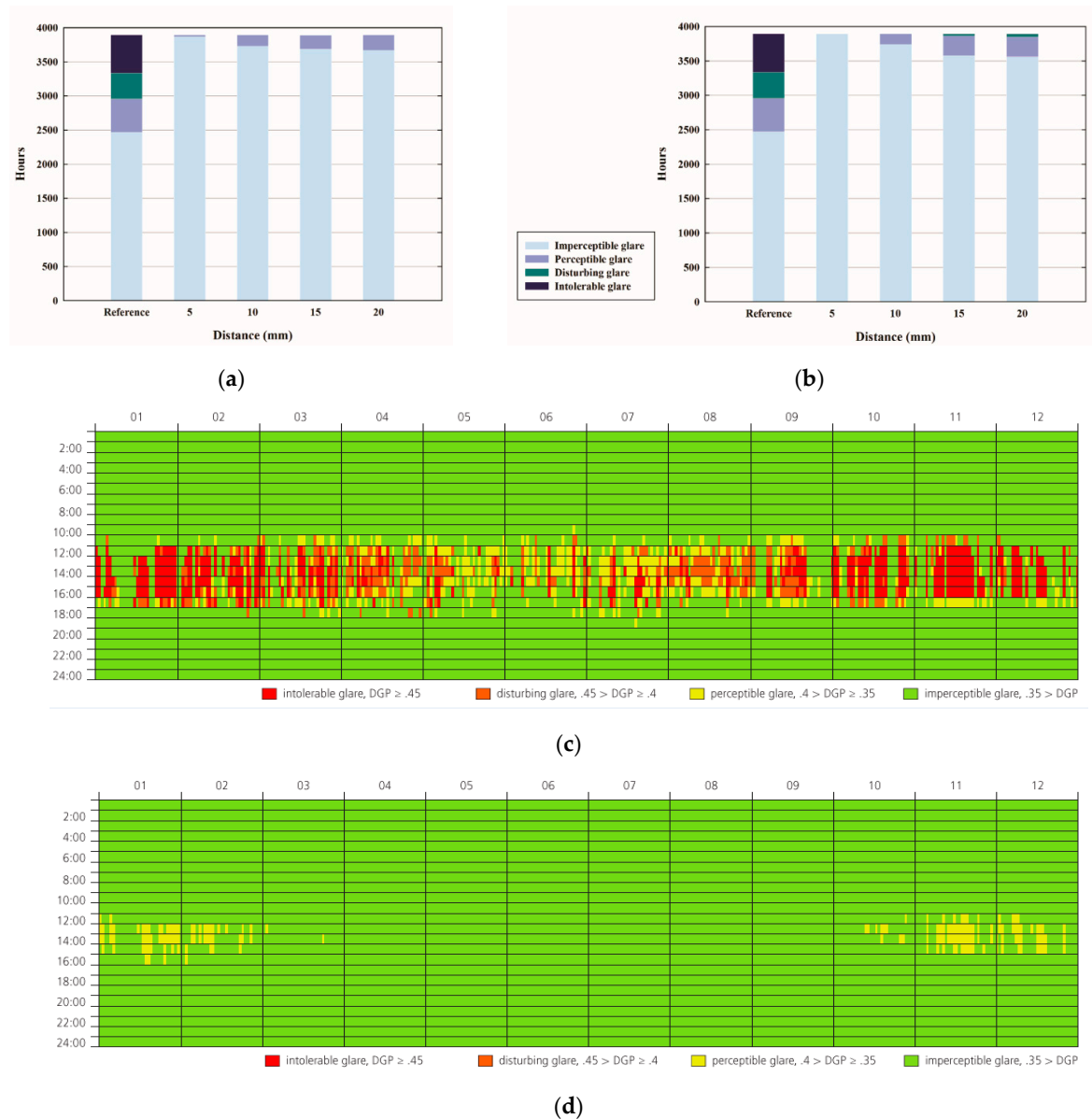
(a)

(b)

(c)

(d)

Figure 11. DGP hours and hourly DGP distribution. (**a**) Hours of DGP for the screens with square sticks. (**b**) Hours of DGP for the screens with round sticks. (**c**) Hourly DGP distribution in a year for the reference room. (**d**) Hourly DGP distribution in a year for the room with a nonuniform woven solar shading screen using square sticks at d = 10 mm.

On the basis of the results in Figure 12a,b, the solar radiation reduction for the summer months or one year could be calculated, indicating the cooling energy saving capacity of the proposed solar screens. With reference to the weather data, the total annual vertical solar insolation was 698.06 kWh/m^2. For the reference room, the annual solar insolation entering the room was 627.45 kWh/m^2. On the basis of Figure 12a,b, the sum of the Q_s values showed that by using different proposed shading screens, the solar insolation gain of a room could be reduced to between 123.37 and 242.06 kWh/m^2 in a year and between 25.82 and 49.99 kWh/m^2 in the summer months (June–August).

The radiation transmittance (τ_s) values of the shading screens for each month are shown in Figure 12c,d. These results were consistent with the results of the DF in Figure 10a,b. For both types of screens, the τ_s value increased gradually as the d value increased. The variations in the τ_s values for different solar screens in a month were well-fitted to a quadratic polynomial. For instance, the quadratic polynomial for the τ_s values of all solar screens with square sticks in August was τ_s = -0.0365d^2 +

1.548d + 7.7291, and the correlation coefficient was 99.7%. Accordingly, the formulas denoted that, in terms of solar radiation control, the smaller the d value was, the better the solar shading performance of the shading screens. However, on the basis of the results of Section 4.1, the DF value was smaller than 2% when the d value was smaller than 8 mm for screens with square sticks or 10 mm for screens with round sticks. Therefore, to achieve a well-balanced performance, the optimal configuration should be the one that meets the DF requirement and reaches the best visual comfort, solar shading, and glare performance possible.
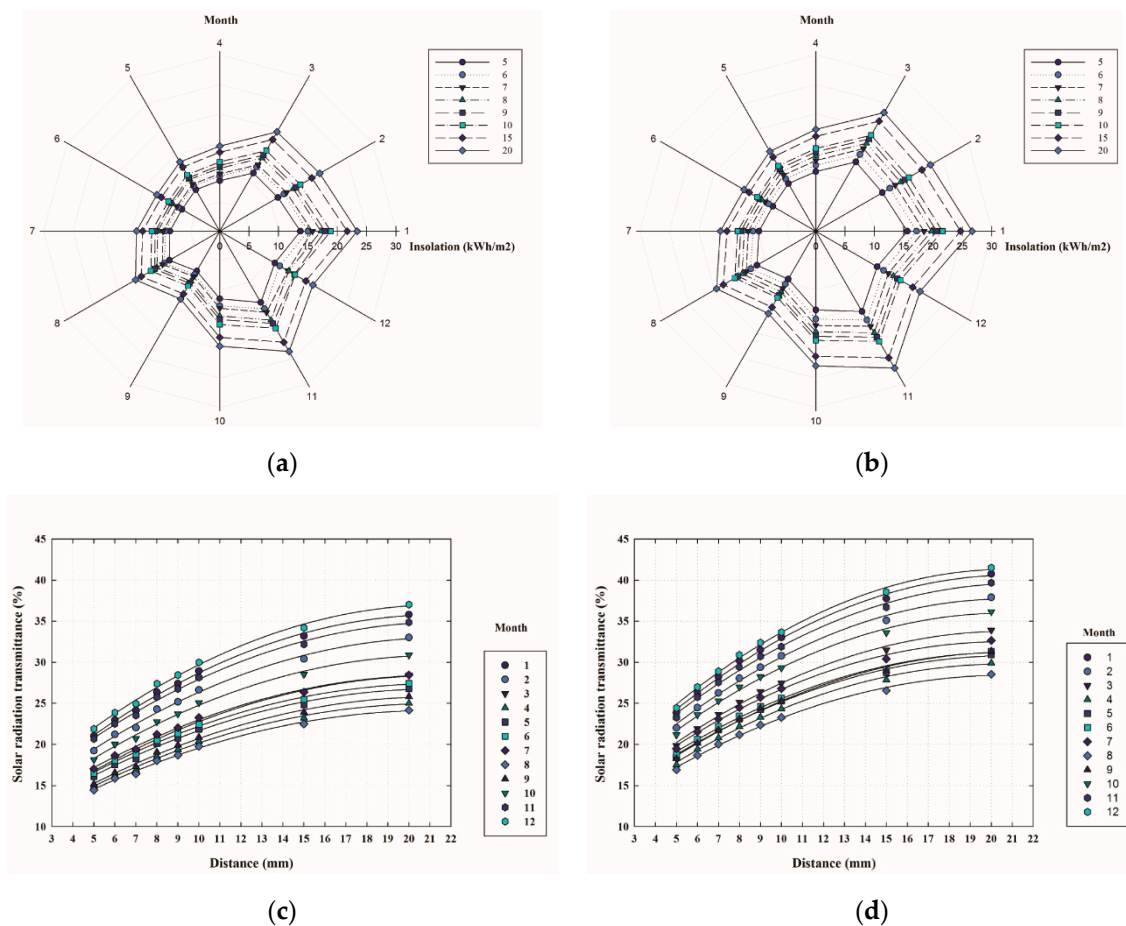

(**a**)   (**b**)

(**c**)   (**d**)

Figure 12. Solar insolation for a room with different solar shading screens and the radiation transmittances for different solar shading screens. (**a**) Solar insolation for a room with screens using square sticks. (**b**) Solar insolation for a room with screens using round sticks. (**c**) Solar radiation transmittances for screens with square sticks. (**d**) Solar radiation transmittances for screens with square sticks.

In summary, the d value of 10 mm is recommended for the screen with square sticks and 8 mm for the screen with round sticks. In these two conditions, the DF values reached 2%, and the $DUI_{100-2000}$ values were close to 100%. Meanwhile, the glare levels were "imperceptible" and "perceptible". These two screen configurations reduced the solar energy gain more than those that achieved the same daylight and glare performances. In addition, their d values were larger than the d value (5 mm) of the estimated panel for mechanical performance in Section 4, and the surface areas exposed to the wind were smaller than the estimated panel, and thus the maximum axial bending stress and deformation of the structures were smaller. As a result, the optimal screens met the strength and stiffness requirements.

5. Conclusions

This study explored external solar shading screens with nonuniform woven panels, which are woven of thick horizontal sticks and thin vertical battens. Integrated simulations and on-site experiments were conducted to calculate the solar optical properties, structural strength, and overall indoor performance of the solar shading screens. A total of 18 solar shading screens with different stick sections and distances between each batten were investigated to optimize the configuration. The primary findings of this study can be summarized as follows:

First, the nonuniform woven bamboo solar shading screen had a preferable overall performance that satisfied the different requirements. For daylighting performance, this screen could completely block the direct visible daylight throughout a summer day (21 June) and allowed 21% horizontal and 28% vertical diffuse daylight to penetrate the room. The solar shading performance reduced up to 100% direct and 79.8% diffuse solar radiation in the summer months. Regarding visual comfort, the screen significantly lowered the glare level, from "disturbing" to "imperceptible", and allowed a basic field view connection to the outdoors through the window. In addition, the proposed woven bamboo panel with a size of 1 × 1 m or smaller withstood a wind load with a speed of 12 m/s. The strength and stiffness, therefore, met the requirements for external solar shading devices.

Second, in terms of optimization, none of the proposed configurations led to an absolute best performance in all respects, including the daylight factor, useful daylight illuminance, glare, and solar energy gain. The optimal configurations in this study exhibited all the factors in balance and achieved better overall performance. For the solar shading screen woven of square sticks and battens, the optimal distance between each batten was 10 mm. For the solar shading screen woven of round sticks and battens, the optimal distance between each batten was 8 mm. Both of the optimal configurations ensured a mean indoor DF greater than 2%, a $DUI_{100-2000}$ near 100%, and a glare level of "imperceptible" or "perceptible". It should be pointed out that the conclusions above were drawn on the basis of the Chinese standards for residential buildings. For other building types with higher or lower requirements on the daylight factor, the optimal configuration might be different. Nevertheless, the optimization method and simulation results presented in this study can assist researchers in conducting further configuration optimization of the proposed solar shading screens for other building types.

In summary, the proposed nonuniform woven solar shading screens can significantly decrease solar energy gain, create a comfortable indoor daylighting environment, and ensure a relatively clear view, as well as meet the mechanical requirements. Furthermore, to support a huge range of scenarios, the solar optical properties of the solar screen in this study can also be applied to nonuniform woven screens made of other materials with similar reflectance values (i.e., reflectance = 0.5 (red), 0.3 (green), 0.2 (blue)), such as wood, rattan, and plastic, or metal with a matte coat. However, the mechanical performance of other materials needs to be evaluated individually.

Abbreviations

Nomenclature

d	distance between each thin batten (mm)
n	safety coefficient
σ_a	allowable stress (kg/cm^2)
σ_b	axial bending stress (kg/cm^2)
σ_p	maximum compressive stress (kg/cm^2)
q_w	wind pressure (kN/m^2)
ρ_a	air density (kg/m^3)
v_w	wind velocity (m/s)
W_a	air gravity (kN/m)
g	gravitational acceleration (m/s^2)
τ_{vh}	horizontal visible daylight transmittances (%)
τ_{vv}	vertical visible daylight transmittances (%)
E_v	outdoor horizontal illuminances (lx)
τ_s	solar radiation transmittance (%)
Q_s	monthly total solar insolation (kWh/m^2)
DGP	daylight glare probability (%)
DF	daylight factor (%)
$UDI_{100-2000}$	useful daylight illuminance with a daylight threshold of 100 to 2000 lx
GL	glare level
CSWD	Chinese standard weather data

Subscript

h	horizontal
v	vertical
o	outdoor
i	indoor
m	mean
dir	direct
dif	diffuse
mon	monthly

References

1. Chiesa, G.; Acquaviva, A.; Grosso, M.; Bottaccioli, L.; Floridia, M.; Pristeri, E.; Sanna, E.M. Parametric Optimization of Window-to-Wall Ratio for Passive Buildings Adopting A Scripting Methodology to Dynamic-Energy Simulation. *Sustainability* **2019**, *11*, 3078. [CrossRef]
2. Knaack, U.; Klein, T.; Bilow, M.; Auer, T. *Façades: Principles of Construction*; Birkhäuser: Basel, Switzerland, 2014.
3. Bellia, L.; Marino, C.; Minichiello, F.; Pedace, A. An overview on solar shading systems for buildings. *Energy Procedia* **2014**, *62*, 309–317. [CrossRef]
4. Hachem, C.; Elsayed, M. Patterns of façade system design for enhanced energy performance of multistory buildings. *Energy Build.* **2016**, *130*, 366–377. [CrossRef]
5. Shen, H.; Tzempelikos, A. Daylighting and energy analysis of private offices with automated interior roller shades. *Sol. Energy* **2012**, *86*, 681–704. [CrossRef]
6. Lu, Y.; Liu, S.W.; Hong, Y.D.; Xiao, Y.Q. Multivariable Optimization of Dynamic Translucent Solar Screen on West-Facing Offices. In Proceedings of the IOP Conference Series: Earth and Environmental Science, Hong Kong, China, 3–5 December 2018; p. 238.
7. Grynning, S.; Lolli, N.; Wågø, S.I.; Risholt, B.D. Solar shading in low energy office buildings-design strategy and user perception. *J. Daylighting* **2017**, *4*, 1–14. [CrossRef]
8. Gratia, E.; De Herde, A. The most efficient position of shading devices in a double-skin facade. *Energy Build.* **2007**, *39*, 364–373. [CrossRef]
9. Atzeri, A.; Cappelletti, F.; Gasparella, A. Internal versus external shading devices performance in office buildings. *Energy Procedia* **2014**, *45*, 463–472. [CrossRef]

10. Dolmans, D.; Hall, A.; Dutoo, G.; Seppänen, O. *Solar Shading: How to Integrate Solar Shading in Sustainable Buildings*; Rehva: Brussels, Belgium, 2010; p. 76.
11. Carletti, C.; Sciurpi, F.; Pierangioli, L. The energy upgrading of existing buildings: Window and shading device typologies for energy efficiency refurbishment. *Sustainability* **2014**, *6*, 5354–5377. [CrossRef]
12. Schittich, C.; Lang, W.; Krippner, R. *Building Skins*; Walter de Gruyter: Berlin, Germany, 2006.
13. Omidfar, A. A methodology for designing contemporary high performance shading screen-the integration of 'form' and the DIVA simulation tool. In Proceedings of the 12th Conference of International Building Performance Simulation Association, Sydney, Australia, 14–16 November 2011.
14. Sherif, A.; El-Zafarany, A.; Arafa, R. External perforated window Solar Screens: The effect of screen depth and perforation ratio on energy performance in extreme desert environments. *Energy Build.* **2012**, *52*, 1–10. [CrossRef]
15. Chi, D.A.; Moreno, D.; Navarro, J. Design optimisation of perforated solar façades in order to balance daylighting with thermal performance. *Build. Environ.* **2017**, *125*, 383–400. [CrossRef]
16. Sabry, H.; Sherif, A.; Gadelhak, M.; Aly, M. Balancing the daylighting and energy performance of solar screens in residential desert buildings: Examination of screen axial rotation and opening aspect ratio. *Sol. Energy* **2014**, *103*, 364–377. [CrossRef]
17. Leung, T.C.Y.; Rajagopalan, P.; Fuller, R. Performance of a daylight guiding system in an office building. *Sol. Energy* **2013**, *94*, 253–265. [CrossRef]
18. Ruck, N.; Aschehoug, O.; Aydinli, S.; Hristoffersen, J.; Courret, G.; Edmonds, I.; Michel, L. *Daylight in Buildings—A Source Book on Daylighting Systems and Components*; Lawrence Berkeley National Laboratory: Berkeley, CA, USA, 2000.
19. Kirimtat, A.; Koyunbaba, B.K.; Chatzikonstantinou, I.; Sariyildiz, S. Review of simulation modeling for shading devices in buildings. *Renew. Sustain. Energy Rev.* **2016**, *53*, 23–49. [CrossRef]
20. Brotas, L.; Rusovan, D. Parametric daylight envelope. In Proceedings of the 29th Conference, Sustainable Architecture for a Renewable Future, Munich, Germany, 10–12 September 2013.
21. Day, J.K.; Futrell, B.; Cox, R.; Ruiy, S.N. Blinded by the light: Occupant perceptions and visual comfort assessments of three dynamic daylight control systems and shading strategies. *Build. Environ.* **2019**, *154*, 107–121. [CrossRef]
22. Lee, B. Heating, Cooling, and Lighting Energy Demand Simulation Analysis of Kinetic Shading Devices with Automatic Dimming Control for Asian Countries. *Sustainability* **2019**, *11*, 1253. [CrossRef]
23. Hensen, J.L.; Lamberts, R. (Eds.) *Building Performance Simulation for Design and Operation*; Routledge: New York, NY, USA, 2012.
24. Nielsen, M.V.; Svendsen, S.; Jensen, L.B. Quantifying the potential of automated dynamic solar shading in office buildings through integrated simulations of energy and daylight. *Sol. Energy* **2011**, *85*, 757–768. [CrossRef]
25. Brownell, B. *Transmaterial 3: A Catalog of Materials That Redefine Our Physical Environment*; Princeton Architectural Press: New York, NY, USA, 2010.
26. Deneyer, A.; Deroisy, B.; Lethé, G.; Flamant, G. Bi-Directional Scattering Distribution Data of Solar Shading: Characterization and Performances. In Proceedings of the CIE Centenary Conference Toward a New Century of Light, Paris, France, 15–16 April 2013.
27. Aljofi, E. The potentiality of reflected sunlight through Rawshan screens. In Proceedings of the International Conference Passive and Low Energy Cooling for the Built Environment, Santorini, Greece, 19–21 May 2005.
28. Iarkus, T.A. The function of windows—A reappraisal. *Build. Sci.* **1967**, *2*, 97–121.
29. Lo, T.Y.; Cui, H.Z.; Tang, P.W.C.; Leung, H.C. Strength analysis of bamboo by microscopic investigation of bamboo fibre. *Constr. Build. Mater.* **2008**, *22*, 1532–1535. [CrossRef]
30. Van der Lugt, P. *Design Interventions for Stimulating Bamboo Commercialization-Dutch Design Meets Bamboo as a Replicable Model*; Delft University of Technology: Delft, The Netherlands, 2008.
31. Dunkelberg, K. *IL-31 Bambus Bambus als Baustoff*; Karl Krämer Verlag: Stuttgart, Germany, 1985.
32. Chang, F.C.; Chen, K.S.; Yang, P.Y.; Ko, C.H. Environmental benefit of utilizing bamboo material based on life cycle assessment. *J. Clean. Prod.* **2018**, *204*, 60–69. [CrossRef]
33. Zea Escamilla, E.; Habert, G.; Correal Daza, J.; Archilla, H.; Echeverry Fernández, J.; Trujillo, D. Industrial or traditional bamboo construction? Comparative Life Cycle Assessment (LCA) of bamboo-based buildings. *Sustainability* **2018**, *10*, 3096. [CrossRef]

34. Liu, W.; Hui, C.; Wang, F.; Liu, G. Review of the Resources and Utilization of Bamboo in China. In *Bamboo–Current and Future Prospects*; Books on Demand: Norderstedt, Germany, 2018; pp. 174–198.

35. Amada, S.; Ichikawa, Y.; Munekata, T.; Nagase, Y.; Shimizu, H. Fiber texture and mechanical graded structure of bamboo. *Compos. Part B Eng.* **1997**, *28*, 13–20. [CrossRef]

36. Lewis, D.; Miles, C.A. *Farming Bamboo*; Lulu: Morrisville, NC, USA, 2007.

37. Vogtländer, J.; van der Lugt, P.; Brezet, H. The sustainability of bamboo products for local and Western European applications. LCAs and land-use. *J. Clean. Prod.* **2010**, *18*, 1260–1269. [CrossRef]

38. Janssen, J.J.A. Designing and building with bamboo. In *China: International Network for Bamboo and Rattan*; Technical University of Eindhoven: Eindhoven, The Netherlands, 2000.

39. Chele, E.S.; Ricardo, M.C.; Ana, P.M.; Teresa, M.R. Bamboo, from traditional crafts to contemporary design and architecture. *Proced. Soc. Behav. Sci.* **2012**, *51*, 777–781. [CrossRef]

40. The Standardization Administration of the People's Republic of China. GB50033; *The People's Republic of China National Standard GB50033—2013: Standard for Daylighting Design of Buildings*; China Standard Press: Beijing, China, 2013. (In Chinese)